A freeze-drying microscopy study of the kinetics of sublimation in a model lactose system

Purnima Ray (née Raman), Chris D. Rielly, Andrew G.F. Stapley*

Department of Chemical Engineering, Loughborough University,

Loughborough, Leicestershire, LE11 3TU, United Kingdom.

*Correspondence:

Dr. Andrew G. F. Stapley

Department of Chemical Engineering, Loughborough University

Loughborough, Leicestershire, LE11 3TU, UK.

Phone: +44-1509-222525

Fax: +44-1509-223923

Email: A.G.F.Stapley@lboro.ac.uk

ABSTRACT

Freeze drying microscopy has been used to probe the lyophilisation kinetics of lactose solutions of various concentrations, at temperatures ranging from -50°C to -30°C and under a constant pressure of 1 Pa. Sublimation front velocities were determined by recording a sequence of video images of the sublimation and analysing the frontal progression using MATLAB. Initial experiments showed poor reproducibility. To combat this, silver iodide (AgI) was added as an ice nucleator, which raised nucleation temperatures and improved reproducibility when compared to non-AgI experiments. The lower supercooling on nucleation when AgI was used also produced larger ice crystals, which enabled the crystal microstructure of the more dilute samples to be more clearly observed. This showed long thin crystals, and the orientation of these crystals with respect to the direction of the frontal movement strongly affected frontal progression rates, which explained the earlier reproducibility problems. A twin resistance mass transfer model, comprising a fixed edge resistance and a resistance which increased with frontal depth, was able to describe the sublimation kinetics. The edge resistance first increased and then decreased with solids content. The resistance per unit depth increased exponentially with solids content, so much so that there is an optimal solids content in relation to the rate of production of dried material. Resistances were also much higher when crystals were oriented with their major axis perpendicular to the direction of frontal movement. Freeze drying rates were approximately proportional to the saturation vapour pressure of water, however the long-held belief that water vapour pressure is the main driving force for mass transfer in freeze-drying systems may be an oversimplification as this only reflects driving forces in the vapour phase (pores) rather than within the solid.

Keywords Lyophilisation; modelling; mass transfer; nucleation; collapse temperature; silver iodide.

1. Introduction

Freeze-drying is a commonly-used technique in the pharmaceutical and food industries for increasing the shelf life and preserving the stability of labile products. Pharmaceutical applications include the freeze-drying of living cells, vaccines, enzymes, and biological media. In the food industry, freeze-drying is applied to the manufacture of products such as coffee, milk powder and infant formula (Chow *et al.*, 2008; Fonseca *et al.,* 2004; Nasirpour *et al.,* 2007; Pardo *et al.,* 2002; Thomas *et al.,* 2004; Yang *et al.,* 2010). The process involves freezing the desired product solution, followed by sublimation and secondary drying (Oetjen, 1999). Sublimation is the primary drying stage of the freeze-drying process, where removal of ice as water vapour takes place at very low temperatures. Secondary drying then follows, where the water is further desorbed from the freeze concentrated solid. As a low temperature process, freeze-drying has the advantage of causing reduced damage compared to higher temperature methods such as spray drying. However it has the disadvantages of being a time and energy intensive process (Tang and Pikal, 2004).

The main steps in a freeze-drying process are the freezing and sublimation steps, which can indirectly and directly influence the cycle duration (Meister *et al.,* 2009). Improvements to the freezing process are often focussed on reducing refrigeration costs. However, the freezing step also determines the internal structure of the frozen material. In particular the rate of freezing influences the size of dendritic and cellular ice crystals. A highly porous structure with reduced diffusional resistance will improve mass and heat transfer during sublimation, thereby reducing the primary drying cycle duration and increasing the overall process efficiency.

Many different methods and devices have been developed over the years to study and improve low temperature freezing and freeze-drying processes (Rosenthal & Rall, 1984; Nail *et al.,* 1994). One such development is freeze-drying microscopy (FDM), which allows the direct visualisation of the sublimation front, as the dried region appears much darker than the

undried icy region (Pikal *et al.*, 1983). Light is transmitted through the icy region with minimal scatter, as the two phases (ice and the freeze concentrated matrix) have similar refractive indices. However, when the ice sublimes to leave voids, the large difference in refractive index between the air pores and the solid matrix causes significant scatter. Thus, the boundary between the two regions is obvious. Ice sublimation only occurs at the front as the microscope slide is firmly sealed to the sample when the (liquid) sample is frozen, and so there is no headspace for the icy region to sublime into other than via the edge of the slide.

The most common current use of FDM is the determination of collapse temperatures (T_c) of products to be freeze-dried. Here, the temperature is allowed to rise as freeze drying progresses. The collapse temperature is defined as the temperature above which loss of structure (or shrinkage) of the product occurs, and is of great importance to an industrial production process as it defines the highest temperature to which the undried frozen product can be exposed without adversely affecting the freeze drying, rehydration properties and storage stability of the sample. Since an increase in temperature can directly increase the productivity by reducing the sublimation time, it can safely be said that T_c is of critical importance to the sublimation process (Pikal and Shah, 1990). Product collapse occurs as a consequence of a transition of the solute phase from the glassy into the rubbery state near the ice-vapour interface, resulting in a decrease in the viscosity of the solute phase and a loss of the porous structure created during the sublimation of ice (Pikal and Shah, 1990).

The freeze-drying microscope allows visualisation of collapse, as the collapsed region is able to transmit light with minimal scatter due to the absence of pores. If the temperature of a freeze drying sample is gradually increased, then a transition from “dark” to “light” will be observed just behind the front as the sample moves through the collapse temperature.

There are many reports in the literature regarding the use of FDM to determine the T_c of various products, for which it is now a well-established technique (Adams and Ramsay, 1996; Meister and Gieseler, 2009; Meister *et al.*, 2009; Yang *et al.,* 2010; Zhai *et al.,* 2003).

However, very few researchers have used FDM to determine frontal velocities or to link them to sublimation rates. This can, in part, be attributed to the time-consuming nature of the analysis, particularly before computational image analysis techniques have become available. For example, Pikal *et al.* (1983) used FDM to study the morphology of the crystal/pore structure produced from different freezing and annealing regimes, but still preferred to use a microbalance technique rather than FDM to study freeze drying kinetics. The first reported use of FDM to determine kinetics appears to be by Kochs *et al.* (1989, 1991), who developed a FDM device which allowed a temperature gradient to be produced across the sample in the initial freezing stage. This resulted in nucleation at one end of the sample and subsequent directional solidification across the sample. Very regularly spaced columnar crystals were produced and the kinetics of the subsequent freeze drying phase could be related to the width of the columnar crystals. Zhai *et al.* (2003) used a commercially available FDM device to study freeze drying kinetics various materials including buffer solutions, a suspension or glass beads and pure ice. The frontal distances varied with the square root of time, and was fitted to a diffusion model (flux proportional to concentration gradient or pressure gradient through the dry layer). The authors characterised the systems in terms of an effective diffusion coefficient through the dry layer. Sublimation times calculated using these D_{eff} values were in broad agreement with the sublimation times in a conventional laboratory vial freeze-dryer for the glass bead system but not for the buffer solutions. This was attributed to cracks appearing in the samples in the vials. It is well known however that the rate of freeze drying is heavily dependent on the microstructure produced by the freezing process, which may be very different between that produced in a vial and that on a microscope slide (Kochs *et al.*, 1989).

The purpose of the current study is to further explore and develop the FDM technique for gaining velocity data of the sublimation front, and in particular how they relate to the porous microstructure. Although very different to conventional systems, this should allow insights to

be gained more generally into freeze drying processes and help understand conventional systems better.

2. Materials and methods

2.1 Materials

α-lactose monohydrate (99.5%), sodium chloride (99.5%), magnesium chloride (>98%), potassium chloride (99%) and silver iodide (AgI, 99%) were purchased from Fisher Scientific/Acros Organics (Loughborough, UK). Sodium chloride, magnesium chloride and potassium chloride were used as eutectic mixtures for the temperature calibration of the microscope stage. Lactose was stored in an air-tight bottle to prevent moisture absorption.

2.2 Determination of Moisture Content

The Karl Fischer titration method was used to determine the moisture content of the as-received *α*-lactose monohydrate (Schuck and Dolivet, 2002). The oven drying or high temperature drying method was not used in this case, as it does not take into account the water present as a hydrate (bound water) in α-lactose monohydrate. The Karl Fischer titration determines the bound as well as unbound water present in samples (Schuck and Dolivet, 2002). The moisture content of the *α*-lactose monohydrate was determined on a wet basis to be 5.8 ± 0.3%.

2.3 Solution preparation

Five different solid concentrations of *α*-lactose monohydrate (5%, 10%, 20%, 30% and 40% w/w) were prepared by dissolving specific masses of lactose powder into a glass sample beaker containing a weighed amount of hot distilled water (70°C). The amount of water to be added to each sample was determined as follows:

$$w = s\left\{\left(\frac{100}{c}\right)-\left(\frac{m}{c}\right)-1\right\} \quad (1)$$

where, *w* is the mass of water to be added (g), *s* is the mass of sample including initial moisture (g), *c* is the final mass percentage solid content of the sample required and *m* is the initial wet basis moisture content of the sample (mass %) determined according to Section 2.2.

2.4 Freeze-drying microscopy

2.4.1 Instrumentation

Experiments were performed using a Linkam FDCS196 variable temperature controlled stage (Linkam Instruments, Tadworth, UK) with an Olympus BX43 microscope (Southend-on-Sea, UK) connected to a QImaging Retiga 2000R digital camera (Surrey, Canada). The stage was sealed so that a vacuum could be drawn using a vacuum pump. The pressure was measured using a Pirani gauge and controlled using an automatic valve over a range of 1 Pa to 100 000 Pa. Samples were mounted on an silver block, the temperature of which was controlled by a combination of liquid nitrogen cooling and electrical heating within the block. The silver block featured a small hole (diameter 1.3 mm) through its centre which allowed illumination of a small part of the sample from a light source below the stage. The stage pressure, temperature and image capture were controlled using Linksys32 software.

2.4.2 Sample preparation

To perform the experiments, 2 µL of sample was loaded on to a circular glass slide (16 mm diameter), with two thin strips of adhesive tape as spacers to achieve a uniform thickness (~30 µm) and covered with another circular glass coverslip (13 mm diameter) which was loaded on to the stage assembly under ambient conditions. The absence of spacers leads to a variation in the thickness of the sample solution thereby further causing potential variations in sublimation front velocity between repeat runs. A drop of silicone oil was used to ensure good thermal contact between the silver block and the bottom of the lower glass slide.

2.4.3 Stage temperature calibration

Calibration of the stage temperature sensor was carried out using 10% solutions (w/w) each of sodium chloride (NaCl), potassium chloride (KCl) and magnesium chloride ($MgCl_2$) (Fonseca *et al.,* 2004; Meister *et al.,* 2009). 2 µL of the salt solution was placed between the microscope slides and loaded on to the stage. The sample was cooled at 10 K min^{-1} and the eutectic freezing temperature of crystal formation (ice and salt crystal) was noted from the images obtained. The deviation in measured temperatures for these transitions were within ±0.3°C of the values published in literature for NaCl (−21.1°C), KCl (−10.7°C) and $MgCl_2$ (−33.6°C) (Meister *et al.,* 2009).

2.4.4 Experimental conditions

Lactose solutions (5, 10, 20, 30 and 40% w/w) were prepared and loaded on to the microscope stage as previously described. Samples were first cooled at one of three different cooling rates (1, 10 and 40 K min^{-1}) to one of three different temperatures (−30°C, −40°C and −50°C) at which point the vacuum pump was turned on to reduce the stage pressure to 1 Pa. This process resulted in the sublimation of ice into water vapour from the sample and movement of the sublimation front was generally observed for about 1000 s. In some cases, the experimental time was extended up to 1 hour to gain better estimates of drying parameters.

For the majority of experiments, a miniscule amount of AgI was placed on the bottom glass slide before loading of the sample. AgI is a nucleating agent for ice (Searles *et al.,* 2001) and was used to induce nucleation at a higher temperature in these samples. The combinations of lactose solid contents, initial cooling rate and final freeze-drying temperatures used in these AgI containing experiments are summarised in Table 1.

To measure the collapse temperature, the sample solution was cooled at 10 K min^{-1} to −40˚C and a vacuum pressure of 1 Pa was applied. Once the vacuum pressure had reached

1 Pa, the sample was heated at a rate of 1 K min^{-1} until structural collapse was observed. The starting point or onset of structural collapse was designated as the collapse temperature (T_c) of the sample.

To prepare samples for examination by scanning electron microscope (see section 2.5), 10% and 40% (w/w) lactose solutions were freeze-dried under the microscope overnight (with and without AgI) in order to obtain fully dried samples.

2.5 Field Emission Gun Scanning Electron Microscopy (FEGSEM)

To study the ice crystal structure of the freeze-dried samples, a Leo 1530VP high resolution field emission gun scanning electron microscope (FEGSEM) (Leo Elektronenskopie GmbH, Oberkochen, Germany) was used at a range of magnifications. The glass slides containing the freeze-dried sample were transferred to a small box containing silica gel in order to minimize contact with room air (to avoid moisture sorption) and immediately taken for the sample preparation process. Initially, a thin layer of Au/Pd coating was sputtered onto the samples via an EMITECH SC7640 Au/Pd sputter coater (Quorum Technologies Ltd, East Grinstead, UK) to provide conduction paths for releasing the excessive surface charges generated during imaging. The sputtering time for Au/Pd coating was 80 s. The imaging of the internal structures was achieved using secondary electrons released from the top surfaces of the samples, which were generated by an incident electron beam with 5 kV accelerating voltage within a working distance of ~15 mm.

2.6 Image analysis of the sublimation front movement

The camera software captured images from the FDM at a rate of 1 every 10 seconds. These images were analysed using an in-house image analysis program developed in MATLAB. The images obtained (see e.g. Fig. 1A) were first calibrated and then thresholded to a user specified value to produce a binary image, with the sublimation front seen as a white band on a black background (Fig. 1B). Optimal threshold values depended on the initial solid

contents of the sample, and were not required to be changed for different repeat runs of the same initial solid content. The user would then define a line parallel to the edge of the sample by defining two pixel points on the first image. A number of lines perpendicular to the sublimation front were then constructed, along which the fronts were to be tracked. Multiple lines were used to ascertain the uniformity of the frontal progression at different positions along the front. Typically, eleven equally spaced lines were used (Fig. 1C). The movement of the sublimation front was then tracked along each line (at the transition from white to black pixels) on each successive image. These pixel points were recorded and converted to frontal distance (μm) which were then plotted as a function of time (s).

2.7 Model of sublimation front movement

A simple mass transfer model was developed to fit the sublimation front position data. In these experiments the sample was very thinly spread between two impermeable glass slides which were in good thermal contact with a temperature-controlled microscope stage. Hence, heat transfer was not considered to be a limiting factor in the progression of the fronts, with the sample essentially being held under uniform and isothermal conditions.

The primary drying rate is thus controlled by mass transfer from the sublimation front, where the water vapour flows through the internal dried region of cross sectional area A and then through the edge layer of the sample. The pump produces a pressure P (1 Pa) at the edge of the sample. It was assumed that water vapour was the only gas in the vapour phase around the sample as the vacuum pump effectively removes all the other gases. At the sublimation front the pressure is equal to the saturation vapour pressure of pure ice (P_{sat}) at the sample temperature. Values for P_{sat} of 38.0 Pa, 12.8 Pa and 3.94 Pa were used, corresponding to freeze drying temperatures of -30°C, -40°C and -50°C respectively (data from Wagner *et al.*, 1994). The difference in pressures ($P_{sat}-P$) is taken as the driving force for mass transfer (Mellor, 1978; Quast and Karel, 1968). The frozen matrix was initially at a uniform moisture content of M_i (dry mass basis), dry solids density (mass of solids per unit

volume) of ρ and dried to a final moisture content of M_f (dry mass basis). The water content of the edge layer of the sample was assumed to be negligible.

Fig. 2 shows the two main types of resistance used in the model, namely, a dense non-porous layer at the edge of the sample and a porous region in the main body of the sample. This gives rise to a fixed resistance (α) corresponding to the edge of the sample and a resistance per unit depth (β) of the porous region, such that the resistance to mass transfer increases linearly with the distance (x) of the sublimation front from the edge of the sample. The presence of a surface layer providing a significant resistance to mass transfer has previously been reported by Quast and Karel (1968).

The mass flux of water vapour perpendicular to the drying front (driving force/resistance) is thus given by,

$$\text{Mass flux} = \frac{P_{sat} - P}{\alpha + \beta x} \tag{2}$$

The mass flux is also related to the sublimation front velocity as follows,

$$\text{Velocity of the front, } v = \frac{dx}{dt} \tag{3}$$

$$\text{Amount of dry solid swept out per unit time} = \frac{\rho A dx}{dt} \tag{4}$$

$$\text{Moisture removed per unit time} = \frac{\rho(M_i - M_f)A dx}{dt} \tag{5}$$

$$\text{Hence, mass flux} = \frac{\rho(M_i - M_f)dx}{dt} \tag{6}$$

Combining equation (2) and equation (6),

$$\frac{\rho(M_i - M_f)dx}{dt} = \frac{P_{sat} - P}{\alpha + \beta x} = \frac{\Delta P}{\alpha + \beta x} \quad (7)$$

This can be more simply expressed as

$$\text{Frontal velocity, } v = \frac{dx}{dt} = \frac{1}{a + bx} \quad (8)$$

where,

$$a = \frac{\alpha\rho(M_i - M_f)}{\Delta P} \text{ and } b = \frac{\beta\rho(M_i - M_f)}{\Delta P} \quad (9)$$

Integrating equation (8) yields (using $x(t=0)=0$),

$$t = ax + \frac{bx^2}{2} \quad (10)$$

Frontal position data were fitted to this equation using least square regression for parameter estimation to obtain the representative 'edge resistance' (*a*) and 'resistance per unit depth of the porous region' (*b*). It can be seen that the quantity (1/*a*) also corresponds to the initial sublimation front velocity. Although it is a dynamic model, the model is not asymptotic as the model assumes a semi-infinite solid combined with a constantly replenishing driving force (ΔP). The model would suggest that the front can theoretically progress for an infinite time, but in practice the front will cease to exist when it has passed through the sample or meets dry material. The above approach differs slightly from that of Zhai *et al.* (2003) in that they did not include a surface resistance term in their model. However, the modelling of the dried layer resistance is equivalent. The parameter β above can be related to the effective diffusivity (D_{eff}) of the dried layer used in Zhai *et al.*'s analysis by:

$$D_{eff} = \frac{\theta RT}{\beta M_w} \quad (11)$$

Where θ is the porosity, R is the Universal Gas Constant, T is temperature, and M_w is the molecular weight of water.

3. Results and discussion

3.1 Experiments without AgI

Fig. 3A inset shows the icy and dry regions of a 10% (w/w) lactose solution frozen without AgI undergoing sublimation in the freeze-drying microscope. The microstructure is evident as there are variations in colour across the sample, although the ice crystals formed are too small to be individually observed, even under high magnification. The frontal progression was reasonably uniform along the length of the front.

Frontal distance versus time plots for the 10% lactose solution are shown in the rest of Fig. 3A. These showed the expected curvature of the plots (which reflects the form of equation 10) with an increase in resistance with frontal depth which slows the sublimation rate over time. However, repeat runs of these experiments were found to show poor reproducibility (see e.g. Fig. 3A), and this was found across all the solid concentrations. Furthermore, nucleation temperatures were also found to vary over a wide temperature range (between −17.3°C and −9.8°C, as shown in both Fig. 3A and Fig. 4). Similar variations in nucleation temperature were found for FDM experiments with sucrose and trehalose by Meister and Gieseler (2009). Thus, the nucleation process is inherently random in this system, although this is true of nucleation in general (Franks, 1998; Searles *et al.,* 2001). A further observation is that when nucleation does occur in the experiments, it produces a very rapid and immediate solidification of the sample. This occurs so quickly that it is almost impossible to catch an image of the solidification process in progress. The differences in nucleation temperature (under identical FDM operating conditions) result in differences in supercooling at the point of nucleation, which has a significant effect on the nucleation rate. Increasing the

supercooling on nucleation results in a larger number of small crystals. It has been widely reported that the freezing profile and the nucleation temperature have a direct effect on the frozen microstructure and subsequent sublimation rate in a freeze drying process (Kochs *et al.* 1991, 1993; Konstantinidis *et al.,* 2011; Patel *et al.*, 2009; Sane and Hsu, 2010; Searles *et al.,* 2001).

In order to overcome this lack of reproducibility, various methods were investigated to control nucleation. These included trying different cooling rates (1, 50, 130 K min^{-1}), and scratching the slides using a metal file (see Fig. 3B) in an attempt to create heterogeneous sites for forced nucleation to occur. However these were unsuccessful.

Methods reported in the literature for controlling ice nucleation include the ice fog technique (Patel *et al.*, 2009) or the addition of *Pseudomonas syringae* (Cochet and Widehem, 2000; Wideham and Cochet, 2003) or silver iodide (AgI) (Clausse *et al.,* 1991; Edwards and Evans, 1960; Edwards *et al.*, 1962; Petzold and Aguilera, 2009; Searles *et al.,* 2001;). The ice-fog technique was discounted as it would be very difficult to achieve under a microscope slide. The addition of *Pseudomonas syringae* was also not preferred due to its biological nature as a pathogen and the extra experimental complexity that using a bacterium entails. Silver iodide, on the other hand, could be easily added to the samples and has a very low solubility (and hence has a negligible effect on the solution thermodynamics), and was thus tried in these experiments.

3.2 Experiments with AgI

The addition of AgI was found to raise and also bring reproducibility to the nucleation temperature (see the reduced error bars in Fig. 4 with AgI, compared to the results without AgI), and so AgI is clearly acting as a nucleation agent. Fig. 4 also shows a steady decrease of nucleation temperature with increasing lactose solid content (for samples with AgI added), which mirrors the freezing point depression effect; for samples without AgI, the effect of solid content on nucleation temperature is masked by the poor reproducibility. All solutions exhibit

a freezing point depression with increasing solid content and nucleation takes place a few degrees below the freezing point temperature thus reached. Previous studies (Whittier, 1932) have reported a freezing point depression of just over 4 K in lactose solutions for 40% (w/w) lactose. This is similar to the variation of nucleation temperature seen here between 5% and 40% (w/w) of approximately 4 K (Fig. 4).

3.3 Microstructure

One consequence of the rise in nucleation temperature from the addition of AgI was that nucleation occurs at a lower degree of subcooling, leading to a lower nucleation rate; thus it was possible to discern individual ice crystals in the frozen sample. Larger crystals result from a decrease in the relative rate of nucleation compared to growth during solidification at the higher temperatures. Long thin ice crystal structures with distinct directionality were observed when compared to non-AgI frozen samples. Various different orientations were observed. Fig. 5A and Fig. 5B show ice crystal orientations that are parallel and perpendicular to the direction of movement of the front, respectively. These crystal orientations were visible only in the case of 5% and 10% (w/w) lactose solutions (Fig. 6A and 6B). As the concentration increased the crystal orientations become less distinct (Fig. 6 C-E) and individual crystals cannot be seen using optical microscopy.

To further examine the sample microstructures, SEM images were taken of freeze dried samples. Fig. 6F shows an SEM image of the edge of a freeze dried 10% lactose sample (under FDM). The pore structure shows evidence of directionality in the crystal structure, as shown in the FDM images of Fig. 6A and B. The porous microstructure did not extend to the very edge of the sample which appears to be relatively non-porous, and provides support for the concept of an edge resistance used in the model, and also reported by earlier workers. A thin surface layer can also be seen in the dried region in Fig. 5A. The thickness of this edge was seen to vary between different runs investigated and which may result in different edge resistances.

Fig. 7 shows scanning electron microscopy (SEM) images obtained at two different magnifications (1KX and 5KX) from 10% and 40% lactose solutions (w/w), both with and without AgI. For most of these samples, the microstructure was too small to be visible under the optical microscope, and so SEM is the only way to examine these samples' microstructures. The SEM images confirmed that the addition of AgI resulted in the formation of larger ice crystals, with more "directionality" and that the crystals were larger in the 10% lactose samples (Fig. 7A-D) than the 40% lactose samples (Fig. 7E-H). The cracks observed in Fig. 7E and Fig. 7G were thought to be due to the removal of the upper coverslip before conducting SEM since no cracks were visible in microscope images of the FDM samples.

3.4 Effect of crystal orientation and concentration on sublimation kinetics

The MATLAB analysis was used in order to determine the frontal position at different points on the same drying front. There were variations in sublimation front velocity due to variations in crystal structure orientations in the same frozen sample; however for a given orientation, highly reproducible results were obtained for repeat experiments (Fig. 8A). The sublimation front movement was observed to move faster through the regions with ice crystals orientated parallel to the front, compared to perpendicular orientations. It is therefore highly plausible that the problems in reproducibility encountered in the non-AgI experiments (Fig. 3) are the consequence of differences in the orientation of the crystal microstructure.

There was much less overall variation between runs when experiments were performed using 40% lactose solutions (Fig. 8B). However, these samples showed less directionality in microstructure when observed by SEM (Fig. 7).

Fig. 8A and B also show least squares fits to the simple mass transfer model. It can be seen that equation (10) generally captures the shape of the graphs well and produces good fits to data, due to the combination of a fixed edge resistance and a porous region resistance which was proportional to depth. Fig. 9 shows the values of α and β calculated using equation (9) from all of the freeze drying experiments performed at −40°C. The original *a*

and *b* data are presented by Raman (2015), and showed the same trends with increasing lactose solid content. (The transformation includes dividing *a* or *b* by $(M_i - M_f)$ to produce α and β respectively, but this did not greatly affect the trends in the data.) The α values were seen to increase for initial solid contents from 5 to 20% (w/w) while decreasing again from 20 to 40% (w/w). The β values were found to increase with increasing solid content all the way from 5 to 40% (w/w). This effect can be attributed to the increase in the sheer quantity of solid material through which the water has to pass. Pikal *et al.* (1983) similarly found from vial/microbalance experiments that mean resistance values increased sharply with solute concentration.

Both α and β values were found to be higher for perpendicular ice crystal orientations than parallel orientations. For β values it can be surmised that the parallel orientation facilitates easier water removal due to the lower number of lactose boundaries per unit distance into the sample, compared to the perpendicular orientation. A detailed study by Kochs *et al.* (1993) found that effective diffusion coefficients (back-calculated from gravimetric and temperature data using a mathematical model) in vial based systems were lower at the bottom of the vial where crystals were equiaxed but higher towards the top of the vial where columnar crystals were present as a result of directional solidification. However, Fig 9 perhaps presents the most direct evidence reported to date of the effect of crystal orientation on sublimation rates.

The lower values for α in the parallel orientation are more difficult to explain, but it has been observed that in the parallel configuration some ice crystals are able to penetrate the surface layer to some extent, and this would reduce the effective edge resistance to mass transfer.

Fig. 10A shows the amount of dry solid produced for different solid contents with time, calculated by multiplying the frontal distance by the dry basis solid density. The solid density values used are shown in Table 2, and do not change during freeze drying. The 40% lactose content shows the fastest production of solid produced, with the 5% (perpendicular) lactose

the slowest. However, at short times frontal distances are most influenced by the surface resistance term. This is evidenced by Table 2 which shows the depths at which the two resistances are equal to each other.

In conventional freeze drying systems, the times and distances are much longer than shown in Fig. 10A, and so predicted values of ρx have been extrapolated in Fig. 10 B for longer times using the previously fitted values of a and b. These show that the best production rate would be achieved by the 10% solution with the crystals oriented parallel to the direction of frontal movement. Good rates were also achieved with 20% and 30% solids contents but less so with 40% and 5% contents. Hence there is clear evidence that intermediate concentrations are optimal. A direct comparison of 10% with 20 and 30% solid contents is difficult due to the lack of an orientation effect with the latter samples, which could practically be induced via directional solidification in conventional freeze drying. Of course, in large scale commercial freeze drying, consideration should also be taken of the energy costs (which are favoured by starting with higher solids contents) as well as production rates.

3.5 Effect of freezing rate

Various cooling rates (2 K min^{-1}, 10 K min^{-1} and 50 K min^{-1}) during freezing were investigated in order to study their effect on freezing and in turn on the subsequent sublimation process via possible changes in the microstructure. Fig. 11 shows the effect of cooling rate on the nucleation temperatures and α and β values for 10% and 40% (w/w) lactose solutions. As expected, the nucleation temperature (Fig. 11A) falls as the cooling rate increases, leading to a greater degree of subcooling at the point of nucleation; the nucleation temperatures are also reduced for higher mass fractions of lactose in the solution, partly as a result of the effects of freezing point depression.

The α values were found to decrease with increases in cooling rate at both lactose contents (Fig. 11B). There are two possible mechanisms for this variation. Firstly, surface evaporation may occur during cooling which would increase the thickness of the surface layer. This

would then be thicker if the cooling rate is slower, as more time is taken to cool the sample. Secondly, the surface layer may be caused by freeze-concentrated liquid becoming expelled from the main body of the sample as ice is formed. There may be more time for liquid to be expelled if cooling rates are lower.

The β values were found to be relatively unaffected by the cooling rate *per se* as seen in Fig. 11C and 11D, despite the significant effect of the cooling rate on the nucleation temperature (Fig. 11A). This contradicts the literature consensus that cooling rate during freezing has a large impact on subsequent freeze drying rates. However, these can be reconciled by noting that cooling rate only affects freeze drying rates indirectly by changing the microstructure. Once microstructure effects are accounted for (see e.g. Fig 11C) then cooling rate itself does not have an impact.

3.6 Effect of freeze drying temperature

Three different final freeze drying temperatures were investigated (−30°C, −40°C and −50°C) for both 10 and 40% (w/w) lactose solutions. Fig. 12 shows initial frontal velocities for 40% lactose solutions at the three different final drying temperatures, and shows an increase with increasing freeze drying temperature. The increase with temperature, however, does not quite match that of the vapour pressure driving force (also shown in Fig. 12).

Fig 13 shows the variation of calculated α and β values with drying temperature. For the case of 10% lactose solutions these were subdivided according to the orientation of the crystals, whereas a single value of α and β is presented for 40% lactose solutions as the microstructures are too small to be distinguishable. In theory, these values should only be mild functions of temperature. Indeed, α values for the parallel orientation of lactose were found to be quite constant for all three final temperatures of drying investigated. However α values were found to increase significantly with increasing drying temperatures for both 10% perpendicular orientation and 40% lactose, which both showed similar values at any given temperature. Some of the differences can be attributed to mass transfer resistances in the

Linkam equipment itself which are the sole contributor to the pure ice values. Local sublimative cooling at the front may also depress the temperature of the subliming ice below that of the controlled (silver block) temperature. This is a possibility particularly since the part of the sample that is observable is not in close contact with the silver block, as it lies above the illumination hole (radius 1.3 mm). A rough calculation, however, indicates that this temperature depression is small (of the order of 0.2 K, this calculation is provided as Supporting Information). It would also be expected that if sublimative cooling was important in this system, that it would affect the fastest drying samples more (i.e. 10% lactose with parallel orientation) whereas this is not the case.

β values shown in Fig 13B, showed large differences based on sample type as seen previously in Fig 9. The parallel/10% lactose data are much smaller than for the other samples and so are shown on an expanded scale in Fig 13C. There were some significant variations in values for the samples which were not monotonic. Although the error bars are quite large they do not account for all of the variation.

The variations seen in *α* and *β* values thus call into question the vapour pressure driving force term used in the model. Current models for mass transfer in porous media involve a number of mechanisms, depending on the phases present. In freeze drying, two phases are possible: the vapour phase within a pore, and the solid phase of the glassy matrix. Liquid phases should not exist unless collapse has occurred, and thus liquid phase related mechanisms, such as capillary flow, can be discounted. Mass transfer within pores will occur by vapour transport such as by Poiseuille (pressure) flow or vapour diffusion (including Knudsen diffusion). However, within the solid matrix, molecular diffusion is likely to be the dominant mechanism. Moisture can transfer between phases by condensation or evaporation of moisture at the pore/wall interfaces. In a typical freeze dried system, almost all the pores will be closed and so mass transfer will have to occur via successive steps: vapour transport across a pore, condensation/adsorption at the pore wall, diffusion through the glassy matrix to another pore, and evaporation into that pore. The literature is universally

agreed that driving forces for vapour transport (whatever the mechanism) are all based on vapour pressure, but diffusion through the solid is usually modelled as driven by either an activity or a concentration gradient (both quantities being related via the sorption isotherm). However, at equilibrium (such as will be approached at a pore/wall interface) the activity depends on the relative humidity (P/P_{sat}) in the adjacent pore headspace (i.e. the vapour pressure referenced to that of pure ice at the same temperature), rather than just the vapour pressure (P). So, a higher temperature in the sample would lead to increase in the vapour pressure generated by the ice interface, but would not increase the relative humidity in the pore, and so the water activity or concentration would not be increased either. This would suggest in that systems where mass transfer is predominantly governed by vapour transport, that drying rates are likely to scale with the vapour pressure driving force (and apparent resistances would appear relatively constant). However, where mass transfer is partly limited by diffusion through the solid matrix, rates would be much less temperature dependent (any dependence would be due to variations of diffusivity with temperature) and apparent resistances would appear to increase with temperature as drying rates failed to keep up with the increase in P_{sat} that ultimately drives mass transfer from the ice interface.

Such a hypothesis could help to explain some of the variations shown in Fig 13. Firstly, the α values showed much greater increases with increasing drying temperature for the 40% and 10% perpendicular samples than with the 10% parallel samples. The argument would be that in the first two cases mass transfer through the surface layer will being almost entirely by diffusion (giving the rise in apparent resistance), whereas in the last case the penetration of the surface layer by the crystal voids would allow some mass transfer to be by vapour transport. The large swings in β values could be a consequence of changes in the relative importance of vapour and solid phase mass transfer.

3.7 Effect of concentration on collapse temperatures

The effect of solid content of lactose solutions (5 to 40%), in the presence of AgI, on the collapse temperature was also investigated. Collapse temperature is determined by the point where the frozen lactose sample starts to lose its structure due to viscous flow as the temperature is increased. The collapsed region appears optically lighter due to the reduction in light scatter as a result of loss of frozen structure, compared to the uncollapsed dried region (darker region) which was dried below the collapse temperature and has remained intact. Fig. 14 (inset) shows the process of structural collapse as seen under FDM; the onset of collapse was measured by observing the light band formation in FDM images obtained while heating the sample and was found to show an increasing trend with increasing solid content (Fig. 14). A similar trend was found by Meister *et al.* (2009) for Polyvinylpyrrolidone solutions. Higher solid content frozen samples were found to be more tolerant of higher temperatures than lower solid contents as they were able to more closely approach the maximally freeze concentrated state. Experiments with non-AgI samples were also conducted for comparison: 10% lactose solution was found to have similar collapse temperatures both with and without AgI; the 30% lactose solutions showed a small variation, however the difference was within ±1 K between AgI and non-AgI samples. Thus the nucleation temperature does not noticeably affect the collapse temperature. Meister *et al.* (2009) found very little correlation between nucleation temperatures and subsequent collapse temperatures.

4. Conclusions

The purpose of this study was to use FDM to gain a better insight into factors such as initial lactose content, freezing rate, and lyophilisation temperature that affect the primary drying phase of the freeze-drying process. Silver iodide was used to induce ice nucleation and was found to bring a consistent pattern to nucleation temperatures, when compared to non-silver

iodide experiments. By also reducing the degree of supercooling on nucleation, the addition of a nucleation agent also meant that crystal sizes were large enough to be observed for dilute (≤10% solids) systems. It is acknowledged that silver iodide cannot be used in food or pharmaceutical industry applications, but its use here allowed better reproducibility of experiments, and suggests that controlling nucleation (which can be achieved via a variety of other means) may result in better overall control of such systems.

Image analysis using MATLAB was applied to sequences of microscope images of the sublimation front to determine the distance travelled by the front over time. The ice crystal size and orientation were found to directly influence the sublimation front velocity. The observed kinetics were also consistent with the presence of a surface layer resistance along with an increasing resistance per unit depth into the porous region. These two regions could also be discerned on microscope and SEM images.

The effects of solid content (5 to 40% w/w), cooling profile (2 K min^{-1}, 10 K min^{-1} and 50 K min^{-1}) and final temperature of drying (−30°C, −40°C and −50°C) on the representative edge resistance (α) and representative resistance of the dried region (β) were also investigated. The representative edge resistance α was found to increase initially with lactose solid content (5, 10 and 20% w/w) followed by a decrease at higher solid contents (30 and 40% w/w), while β values were found to strongly increase with increasing solid content. The amount of dried solid lactose produced with time was initially found to be higher with an initial lactose content of 40% than 5% lactose, but extrapolated data show the existence of an optimal lactose content. Cooling rates (2 K min^{-1}, 10 K min^{-1} and 50 K min^{-1}) were mainly found to affect the surface resistance and this may be due to different levels of surface drying when the samples are being cooled for different lengths of time. Freeze drying rates also increased with increasing temperature, approximately in line with the vapour pressure of water which is widely held to constitute the main driving force for mass transfer in freeze drying systems. However the fitted values of the two resistances showed sizeable variations with temperature whereas they would be expected to be more constant. This may be due in

some cases to diffusion through the solid walls of the porous structure playing a significant role, as this is driven by activity or concentration differences rather than vapour pressure.

A greater understanding of the effect of the structure of the frozen matrix on the freeze-drying process has also been achieved. It has been conclusively demonstrated that an edge resistance has a significant effect on sublimation rates (at least at short times) and the size and orientation of ice crystals plays a significant role in determining sublimation front velocities. Ice crystals parallel to the direction of sublimation were found to have faster sublimation front velocities and the larger ice crystals in AgI containing samples facilitated faster front movement.

Acknowledgement

The authors would like to thank the Department of Chemical Engineering, Loughborough University, UK for funding this work.

References

Adams, G. D. J., Ramsay, J. R., 1996. Optimizing the lyophilization cycle and the consequences of collapse on the pharmaceutical acceptability of *Erwinia* L-Asparaginase. Journal of Pharmaceutical Sciences, 85, 1301-1305.

Chow, K. T., Zhu, K., Tan, R. B. H., Heng, P. W. S., 2008. Investigation of electrostatic behaviour of a lactose carrier for dry powder inhalers. Pharmaceutical Research, 25, 2822-2834.

Clausse, D., Bouabdillah, D., Cochet, N., Luquet, M. P., Pulvin, S., 1991. Ice crystallization induced by silver iodide and bacteria in microsize droplets dispersed within emulsions. Pure and Applied Chemistry, 63, 1491-1494.

Cochet, N., Widehem, P., 2000. Ice crystallization by *Pseudomonas syringae*. Applied Microbiology and Biotechnology, 54, 153-161.

Edwards, G. R., Evans, L. F., 1960. Ice nucleation by silver iodide: I. Freezing vs sublimation. Journal of Meteorology, 17, 627-634.

Edwards, G. R., Evans, L. F., La Mer, V. K., 1962. Ice nucleation by monodisperse silver iodide particles. Journal of Colloid Science, 17, 749-758.

Fonseca, F., Passot, S., Cunin, O., Marin, M., 2004. Collapse temperature of freeze-dried *Lactobacillus bulgaricus* suspensions and protective media. Biotechnology Progress, 20, 229-238.

Franks, F., 1998. Freeze-drying of bioproducts: putting principles into practice. European Journal of Pharmaceutics and Biopharmaceutics, 45, 221–229.

Kochs, M., Schwindke, P., Korber, C., 1989. A Microscope Stage for the Dynamic Observation of Freezing and Freeze-Drying in Solutions and Cell-Suspensions. Cryo-Letters, 10, 401-420.

Kochs, M., Korber, C., Nunner, B., Heschel, I., 1991. The Influence of the Freezing Process on Vapor Transport During Sublimation in Vacuum-Freeze-Drying. International Journal of Heat and Mass Transfer, 34, 2395-2408.

Kochs, M., Korber, C., Heschel, I., Nunner, B., 1993. The Influence of the Freezing Process on Vapor Transport During Sublimation in Vacuum-Drying Freeze-Drying of Macroscopic Samples. International Journal of Heat and Mass Transfer 36, 1727-1738.

Konstantinidis, A. K., Kuu, W., Otten, L., Nail, S. L., Sever, R. R., 2011. Controlled nucleation in freeze drying: Effects on pore size in the dried product layer, mass transfer resistance and primary drying rate. Journal of Pharmaceutical Sciences, 100, 3453-3470.

Meister, E., Sasic, S., Gieseler, H., 2009. Freeze-dry microscopy: Impact of nucleation temperature and excipient concentration on collapse temperature data. AAPS: PharmSciTech, 10, 582-588.

Meister, E., Gieseler, H., 2009. Freeze-dry microscopy of protein/sugar mixtures: Drying behaviour, interpretation of collapse temperature and a comparison to corresponding glass transition data. Journal of Pharmaceutical Sciences, 98, 3072-2087.

Mellor, J.D., 1978. Fundamentals of Freeze Drying. Academic Press, London.

Nail, S. L., Her, L-M, Proffitt, P. B., Nail, L. L., 1994. An improved microscope stage for direct observation of freezing and freeze drying. Pharmaceutical Research, 11, 1098-1100.

Nasirpour, A., Landillon, V., Cuq, B., Scher, J., Banon, S., Desorby, S., 2007. Lactose crystallization delay in model infant foods made with lactose, β-Lactoglobulin and starch. Journal of Dairy Science, 90, 3620-3626.

Oetjen, G. W., 1999. Freeze Drying, Wiley-VCH, Weinheim, Germany.

Pardo, J. M., Suess, F., Niranjan, K., 2002. An investigation into the relationship between freezing rate and mean ice crystal size for coffee extracts. Food and Bioproducts Processing, 80, 176-182.

Patel, S. M., Bhugra, C., Pikal, M. J., 2009. Reduced pressure ice fog technique for controlled ice nucleation during freeze-drying. AAPS PharmSciTech, 10, 1406-1411.

Petzold, G., Aguilera, J. M., 2009. Ice morphology: Fundamentals and technological applications in foods. Food Biophysics, 4, 378-396.

Pikal, M.J., Shah, S., Senior, D., Lang, J.E., 1983. Physical-chemistry of freeze-drying - measurement of sublimation rates for frozen aqueous solutions by a microbalance technique. Journal of Pharmaceutical Sciences, 72, 635-650.

Pikal, M. J., Shah, S., 1990. The collapse temperature in freeze drying: Dependence on measurement methodology and rate of water removal from the glassy phase. International Journal of Pharmaceutics, 62, 165-186.

Quast, D. G., Karel, M., 1968. Dry Layer Permeability and Freeze-Drying Rates in Concentrated Fluid Systems. Journal of Food Science 33, 170-175.

Raman, P. 2015, Freeze Drying Microscopy as a Tool to Study Sublimation Kinetics, PhD. Thesis, Loughborough University.

Rosenthal, M., Rall, W. F., 1984. Digital temperature controller for low-temperature light microscopy. Medical & Biological Engineering & Computing, 22, 471-474.

Sane, S. U., Hsu, C.C., 2010. Considerations for Successful Lyophilization Process Scale-Up, Technology Transfer, and Routine Production, in: Jameel, F., Hershenson S., (Eds.), Formulation and Process Development Strategies for Manufacturing Biopharmaceuticals. John Wiley & Sons, Inc., Hoboken, NJ, pp.797-826.

Schuck, P., Dolivet, A., 2002. Lactose crystallization: determination of α-lactose monohydrate in spray dried dairy products. Lait: EDP Sciences, 82, 413-421.

Searles, J. A., Carpenter, J. F., Randolph, T. W., 2001. The ice nucleation temperature determines the primary drying rate of lyophilisation for samples frozen on a temperature-controlled shelf. Journal of Pharmaceutical Sciences, 90, 860-871.

Tang, X., Pikal, M. J., 2004. Design of freeze drying processes for pharmaceuticals: Practical advice. Pharmaceutical Research, 21, 191-200.

Thomas, M. E. C., Scher, T. J., Desorby, S., 2004. Lactose/β-Lactoglobulin interaction during storage of model whey powders. Journal of Dairy Science, 87, 1158-1166.

Wagner, W., Saul, A., Pruss, A., 1994. International Equations for the Pressure along the Melting and along the Sublimation Curve of Ordinary Water Substance. Journal of Physical and Chemical Reference Data, 23, 515-525.

Whittier, E. O., 1932. Freezing Points and Osmotic Pressures of Lactose Solutions. Journal of Physical Chemistry, *37*, 847–849.

Widehem, P., Cochet, N., 2003. *Pseudomonas syringae* as an ice nucleator – application to freeze-concentration. Process Biochemistry, 39, 405-410.

Yang, G., Gilstrap, K., Zhang, A., Xu, L. X., He, X., 2010. Collapse temperature of solutions important for lyopreservation of living cells at ambient temperature. Biotechnology and Bioengineering, 106, 247-259.

Zhai, S., Taylor, R., Sanches, R., and Slater, N. K. H., 2003. Measurement of lyophilisation primary drying rates by freeze-drying microscopy. Chemical Engineering Science, 58, 2313-2323.

Table 1 Lactose solid contents, cooling rates during freezing and final temperatures of drying studied in the presence of Silver iodide (AgI)

Solid Content (% w/w)	Cooling profile (K min^{-1})	Final drying temperature (ºC)
5	10	-40
10	2	-40
	10	-30, -40, -50
	50	-40
20	10	-40
30	10	-40
40	2	-40
	10	-30, -40, -50
	50	-40

Table 2 Lactose solid content, depth (*x,* where *a* = *b x*) calculated using frontal distance with time and and dry solid density in the presence of Silver iodide (AgI)

Solid Content (% w/w)	Depth (mm)		Dry solid density (kg m^{-3})
	Parallel orientation	Perpendicular orientation	
5	3.32	1.10	50.3
10	1.15	0.32	103
20	0.19		215
30	0.072		331
40	0.021		465

List of Figures

Figure 7. Scanning electron microscope images of freeze dried samples: A and C. 10% lactose initial concentration freeze dried without AgI (1KX and 5KX magnification). B and D. 10% lactose initial concentration freeze dried with AgI (1KX and 5KX). E and G. 40% lactose initial concentration freeze dried without AgI (1KX and 5KX). F and H. 40% lactose initial concentration freeze dried with AgI (1KX and 5KX).

Figure 8. A. Frontal distances vs time for parallel and perpendicular crystal orientations of 5% w/w lactose samples (with AgI), frozen at a cooling rate of 10 K min^{-1} and freeze dried at -40ºC and 1 Pa. B. Frontal distances vs time of 40% w/w lactose samples (with AgI) frozen at a cooling rate of 10 K min^{-1} and freeze dried at -40ºC and 1 Pa. Each data point corresponds to the mean value of at least 5 pixel points from the multiple line analysis. Also shown (solid lines) are fits to the twin resistance model.

Figure 9. Variation with lactose content of A. edge resistance α, and B resistance of dried layer β, for samples containing AgI cooled at 10 K $min^{-1}$and freeze dried at −40ºC and 1 Pa.

Figure 10. Mass of dried solid per unit frontal area (ρx) versus time for samples containing AgI with different initial solid contents of lactose cooled at 10 K min^{-1} and freeze dried at −40ºC and 1 Pa. A. Based directly on experimental data, B. Extrapolated to longer times using experimental *a* and *b* values.

Figure 11. Effect of freezing at three different cooling rates (2, 10 and 50 K min^{-1}) on A. Nucleation temperatures of 10% and 40% lactose solutions frozen at −40˚C with AgI. B. Edge resistance α, of 10% and 40% (w/w) lactose solutions (both containing AgI) and C. and D. Resistance of dried layer β, of 10% and 40% (w/w) lactose solutions respectively. 10% lactose data are divided into parallel and perpendicular ice crystal structures.

Figure 12. Initial sublimation front velocity versus freeze drying temperature for ice and 10% and 40% lactose solutions. Also plotted for comparison (using right hand y-axis) is the vapour pressure difference driving force ($P_{sat} - P$).

Figure 13. Effect of freeze drying temperature on fitted resistance values for 10% (w/w) (both parallel and perpendicular ice crystal structures) and 40% (w/w) lactose systems. A. edge resistance (also compared with value for ice), B. resistance of dried layer per unit depth, C. with expanded scale to better show 10% (w/w) lactose (parallel orientation) data.

Figure 14. Variation of collapse temperature with solid content of lactose, with and without AgI, frozen at a cooling rate of 10 K min^{-1} to -40°C, and freeze dried at 1 Pa whilst heating at 1 K min^{-1}. Inset - Structural collapse observed in a 10% w/w lactose sample with AgI after freezing at a cooling rate of 10 K min^{-1} to -40°C, and during freeze drying at 1 Pa whilst heating at 1 K min^{-1}.

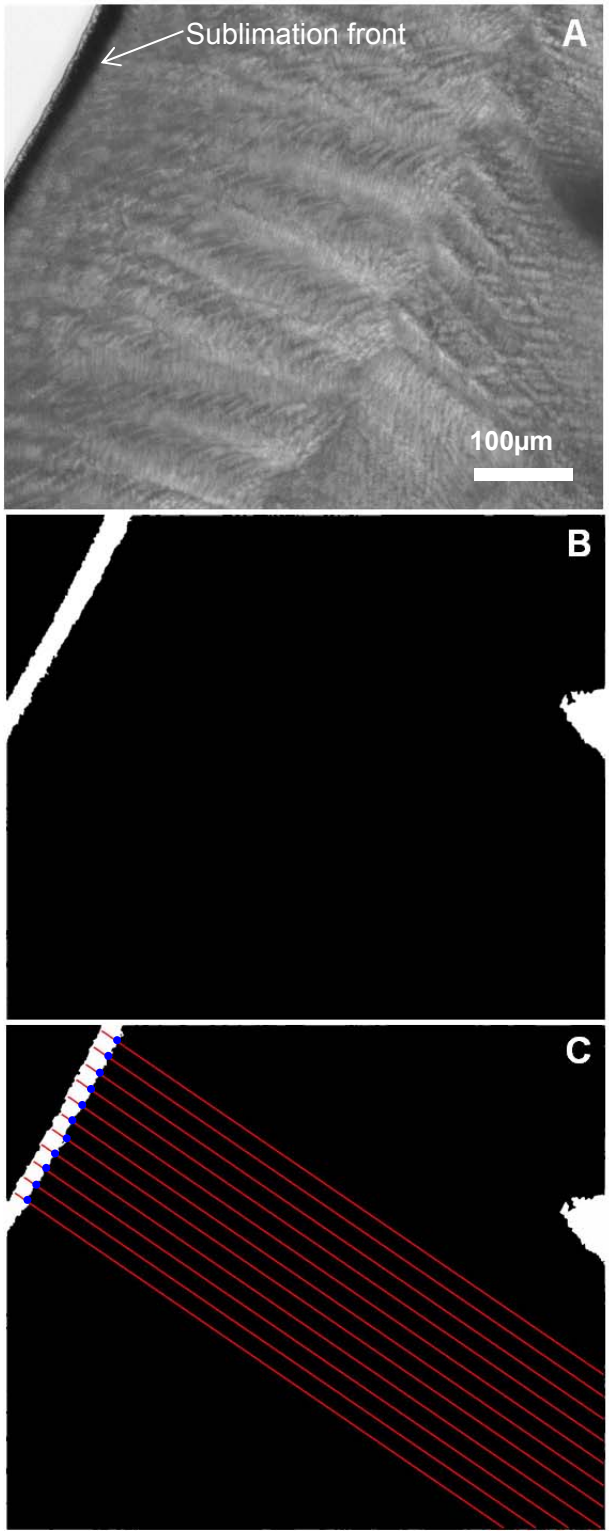
Sublimation front
A
100µm
B
C

Figure 1

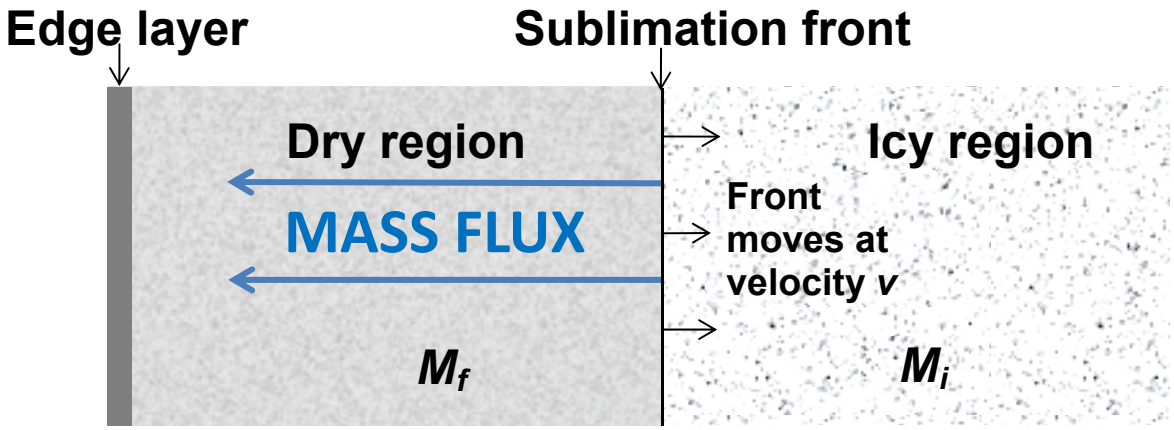
Edge layer
Sublimation front
Dry region
Icy region
MASS FLUX
Front
moves at
velocity v
M_f
M_i

Figure 2

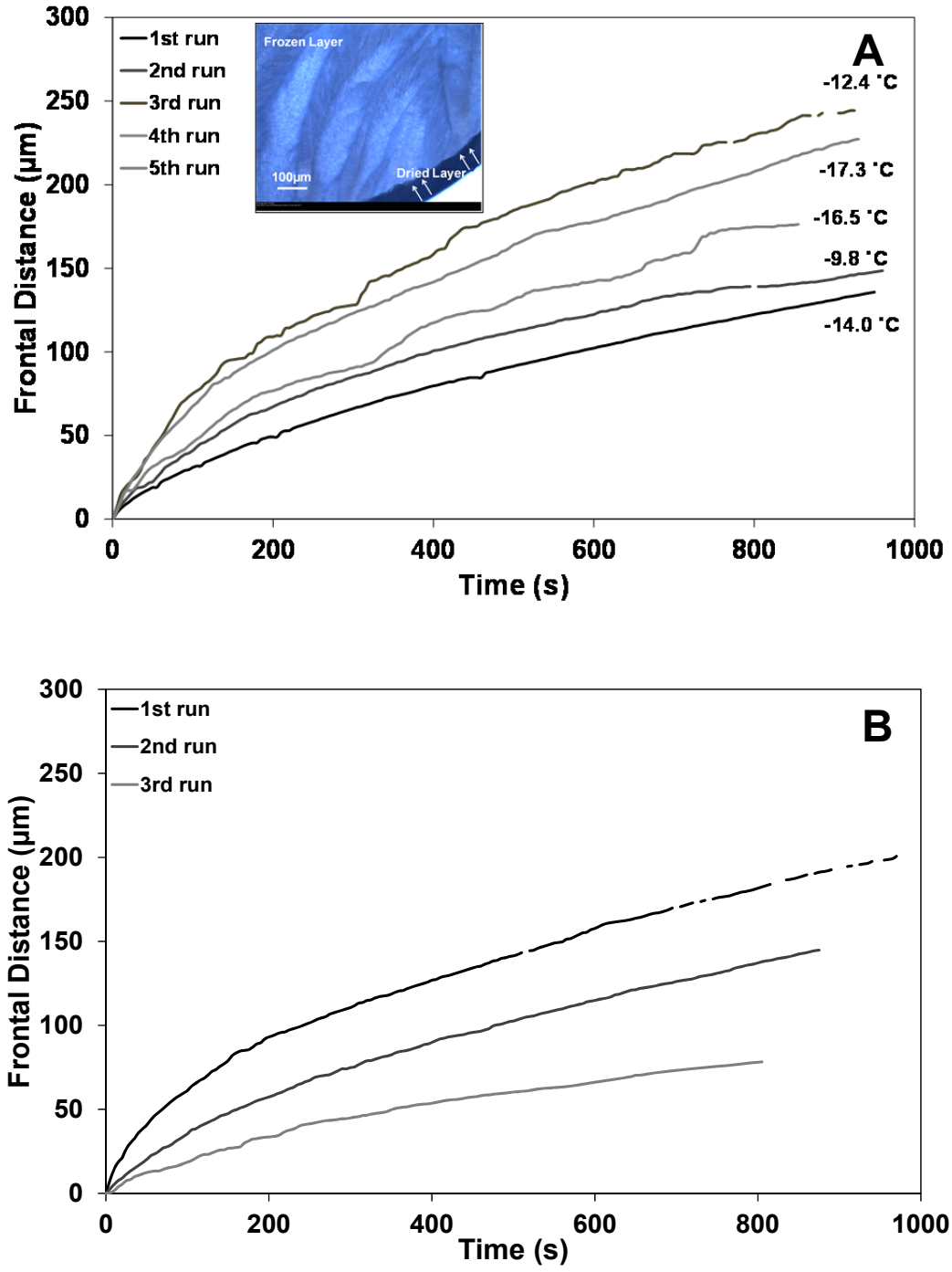
A
1st run
2nd run
3rd run
4th run
5th run
Frozen Layer
Dried Layer
100µm
-12.4 °C
-17.3 °C
-16.5 °C
-9.8 °C
-14.0 °C
Frontal Distance (µm)
Time (s)
0
50
100
150
200
250
300
0
200
400
600
800
1000
B
1st run
2nd run
3rd run
Frontal Distance (µm)
Time (s)

Figure 3

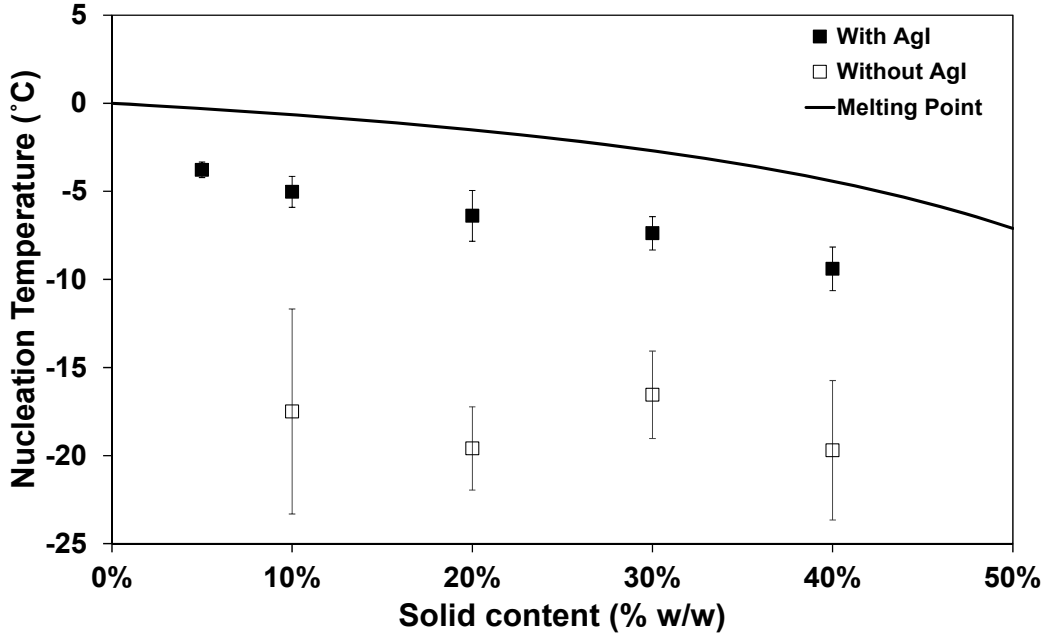
5
0
-5
-10
-15
-20
-25
Nucleation Temperature (˚C)
0%
10%
20%
30%
40%
50%
Solid content (% w/w)
With AgI
Without AgI
Melting Point

Figure 4

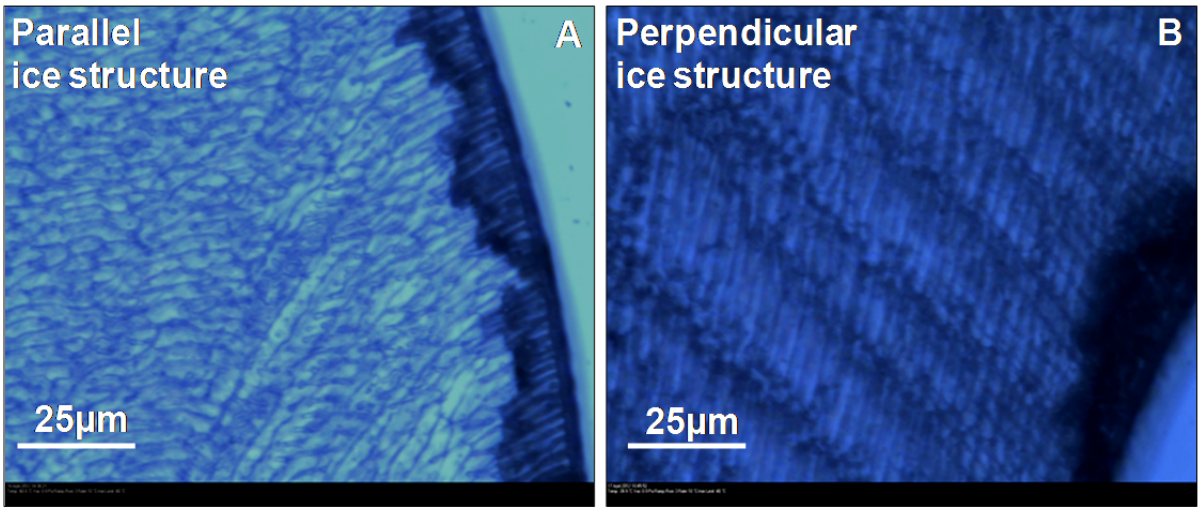
Parallel
ice structure
A
25µm
Perpendicular
ice structure
B
25µm

Figure 5

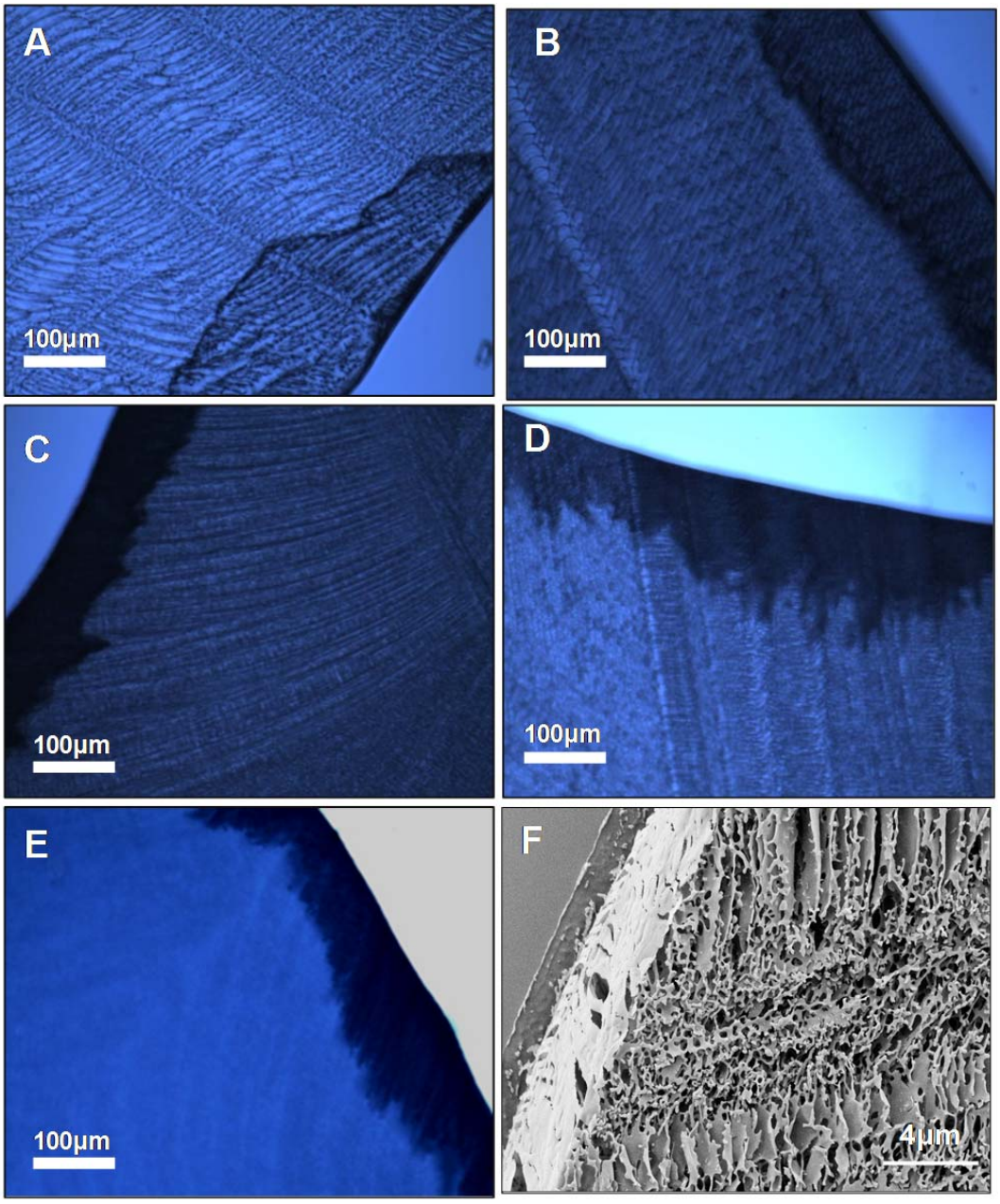

Figure 6

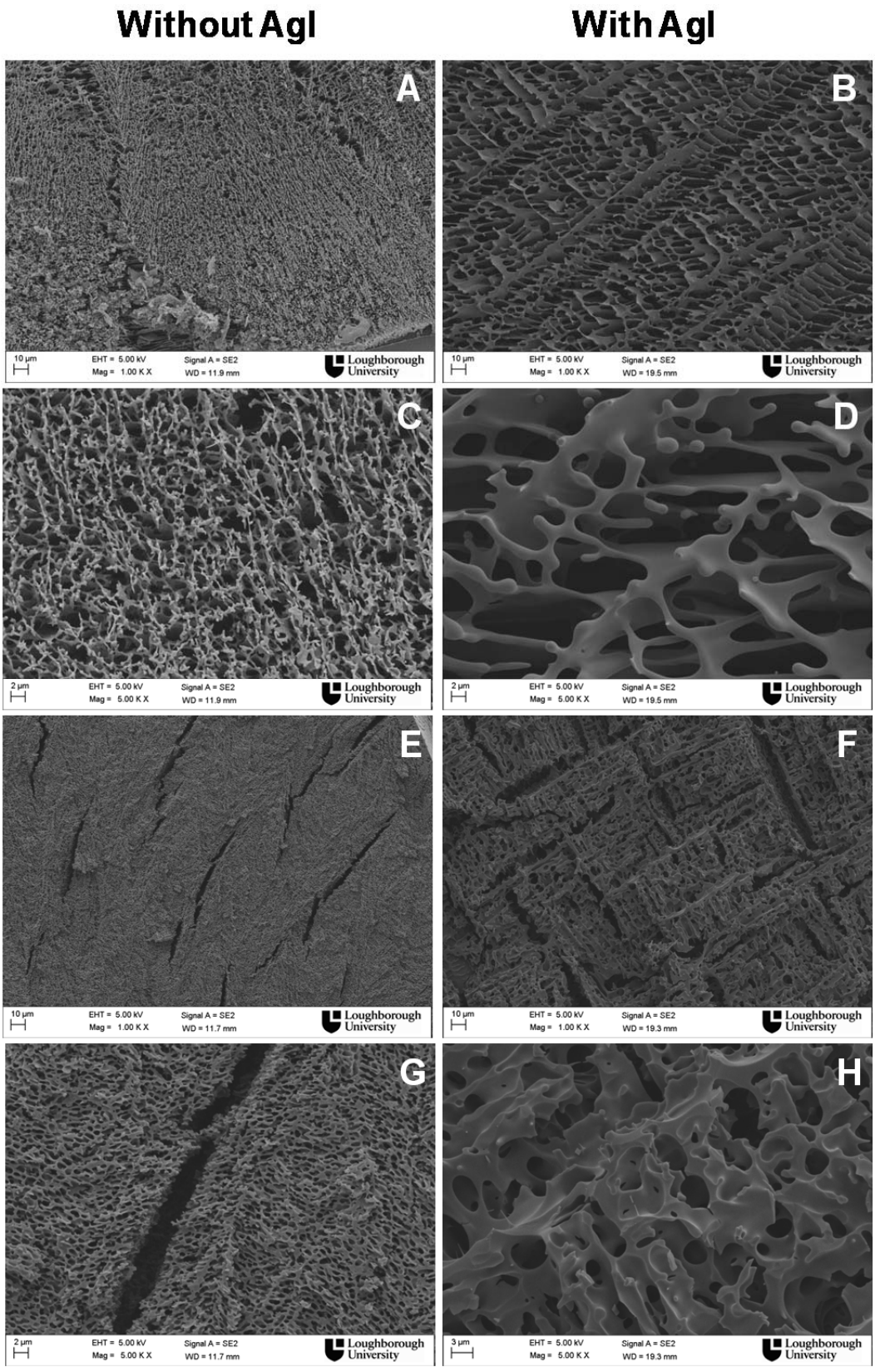
Without AgI
With AgI
A
B
C
D
E
F
G
H
10 µm
EHT = 5.00 kV
Mag = 1.00 K X
Signal A = SE2
WD = 11.9 mm
WD = 19.5 mm
2 µm
Mag = 5.00 K X
WD = 11.7 mm
WD = 19.3 mm
3 µm
Loughborough University

Figure 7

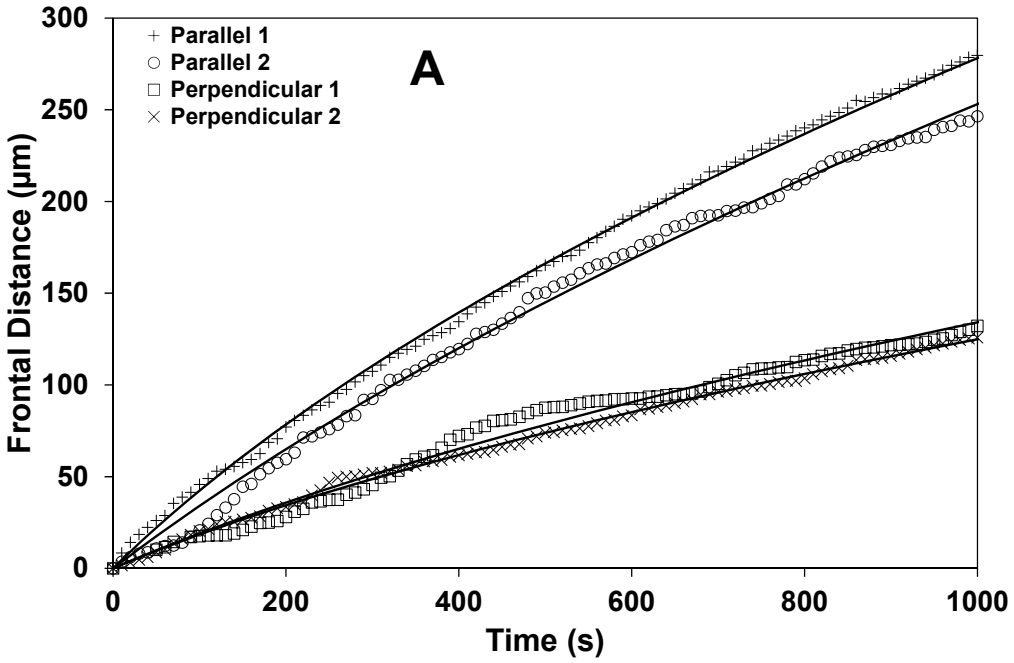
A
Parallel 1
Parallel 2
Perpendicular 1
Perpendicular 2
Frontal Distance (µm)
Time (s)
0
50
100
150
200
250
300
0
200
400
600
800
1000

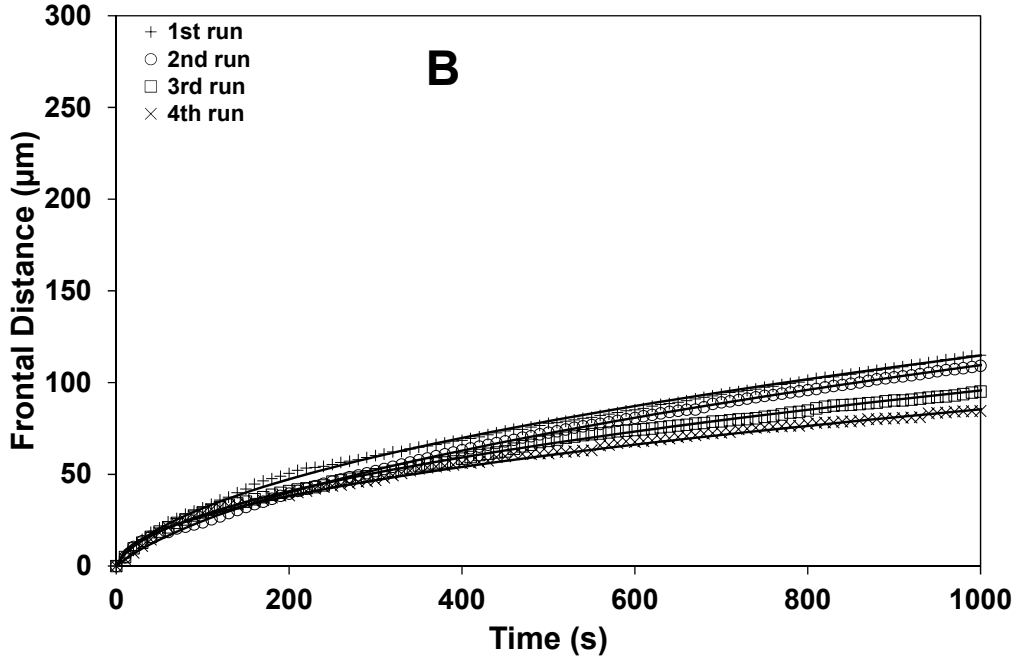
B
1st run
2nd run
3rd run
4th run
Frontal Distance (µm)
Time (s)
0
50
100
150
200
250
300
0
200
400
600
800
1000

Figure 8

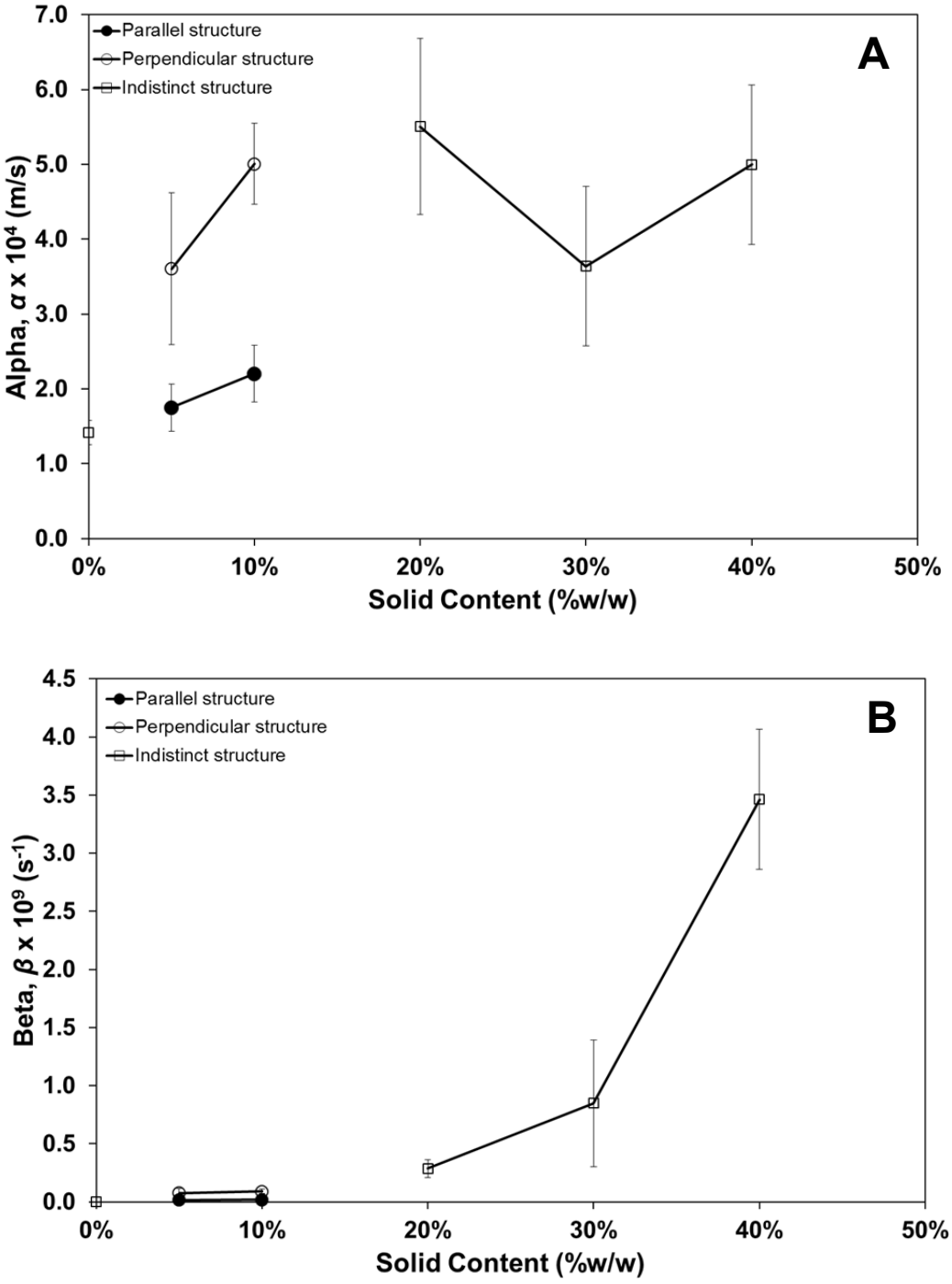
A
Parallel structure
Perpendicular structure
Indistinct structure
Alpha, α x 10⁴ (m/s)
7.0
6.0
5.0
4.0
3.0
2.0
1.0
0.0
0%
10%
20%
30%
40%
50%
Solid Content (%w/w)
B
Parallel structure
Perpendicular structure
Indistinct structure
Beta, β x 10⁹ (s⁻¹)
4.5
4.0
3.5
3.0
2.5
2.0
1.5
1.0
0.5
0.0
0%
10%
20%
30%
40%
50%
Solid Content (%w/w)

Figure 9

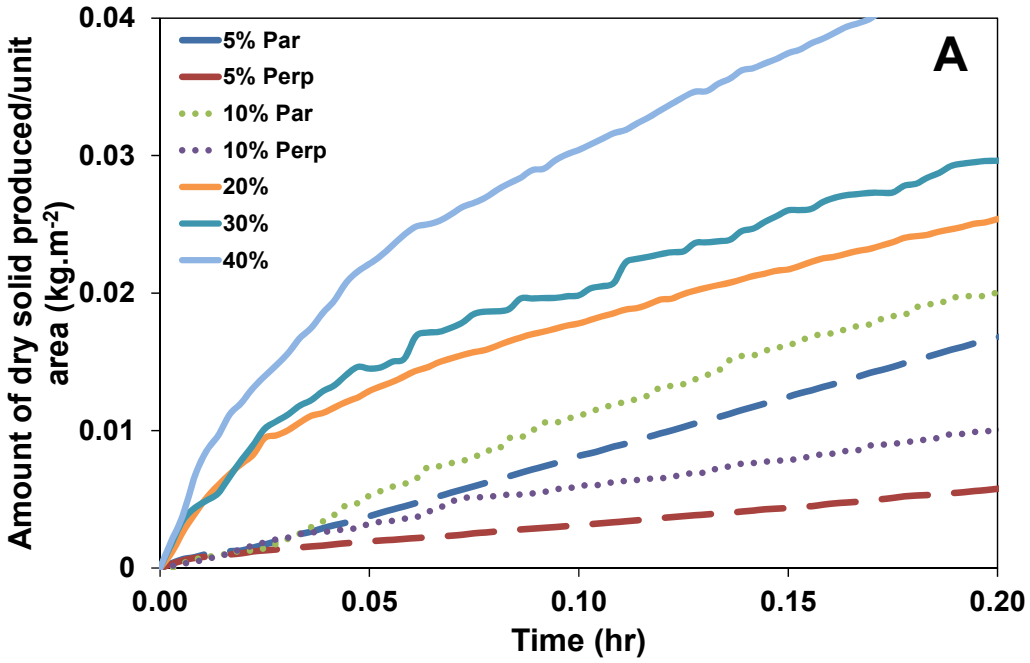
A
5% Par
5% Perp
10% Par
10% Perp
20%
30%
40%
Amount of dry solid produced/unit area (kg.m-2)
0.04
0.03
0.02
0.01
0
0.00
0.05
0.10
0.15
0.20
Time (hr)

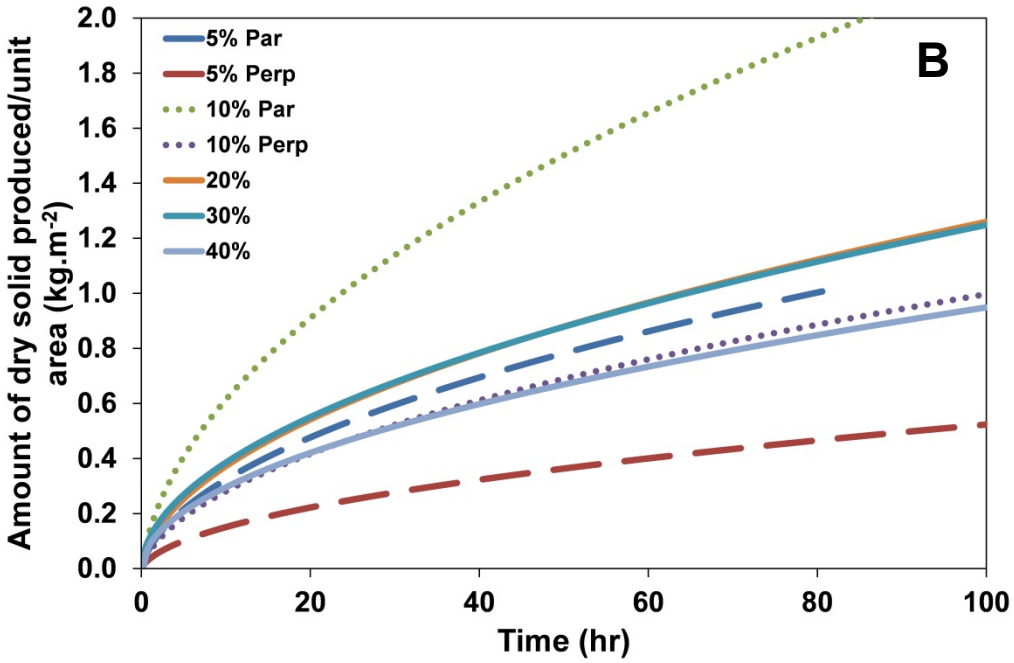
B
5% Par
5% Perp
10% Par
10% Perp
20%
30%
40%
Amount of dry solid produced/unit area (kg.m-2)
2.0
1.8
1.6
1.4
1.2
1.0
0.8
0.6
0.4
0.2
0.0
0
20
40
60
80
100
Time (hr)

Figure 10

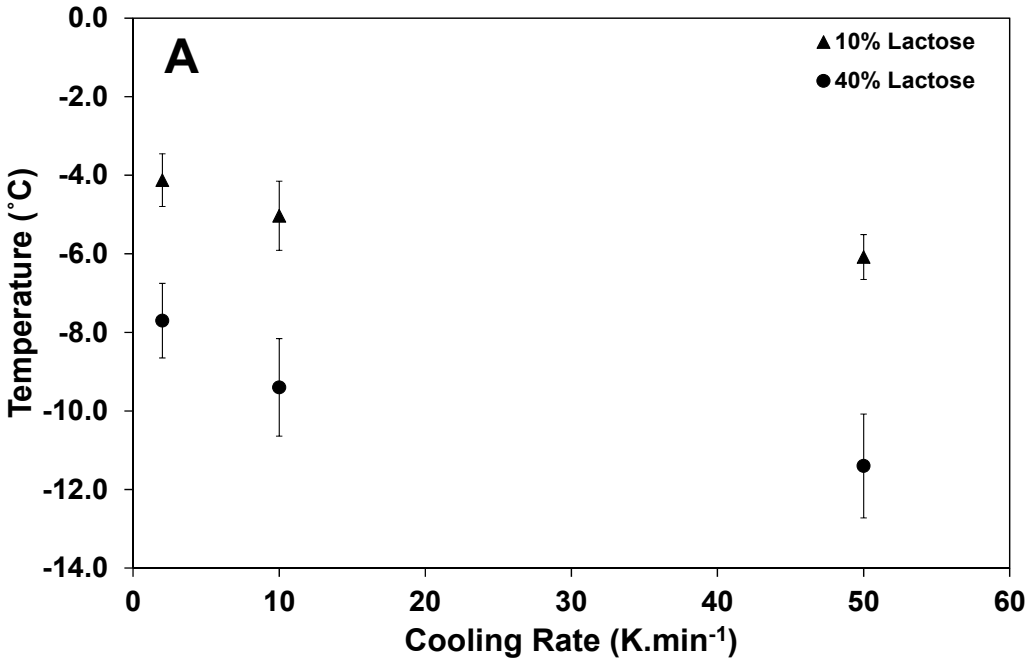
A
10% Lactose
40% Lactose
Temperature (°C)
0.0
-2.0
-4.0
-6.0
-8.0
-10.0
-12.0
-14.0
0
10
20
30
40
50
60
Cooling Rate (K.min-1)

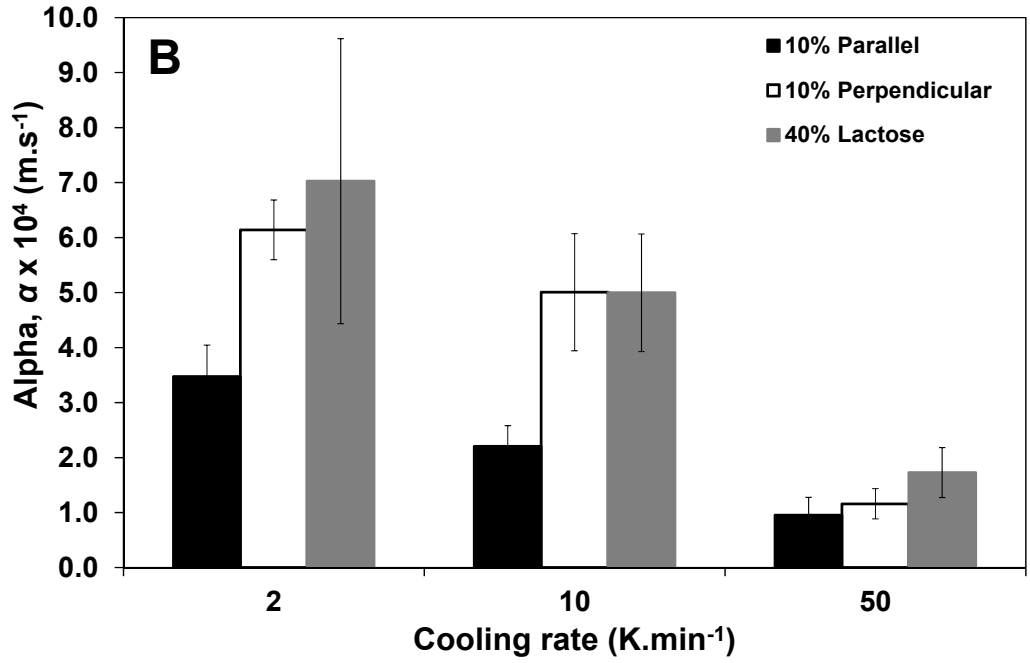
B
10% Parallel
10% Perpendicular
40% Lactose
Alpha, α x 10⁴ (m.s-1)
10.0
9.0
8.0
7.0
6.0
5.0
4.0
3.0
2.0
1.0
0.0
2
10
50
Cooling rate (K.min-1)

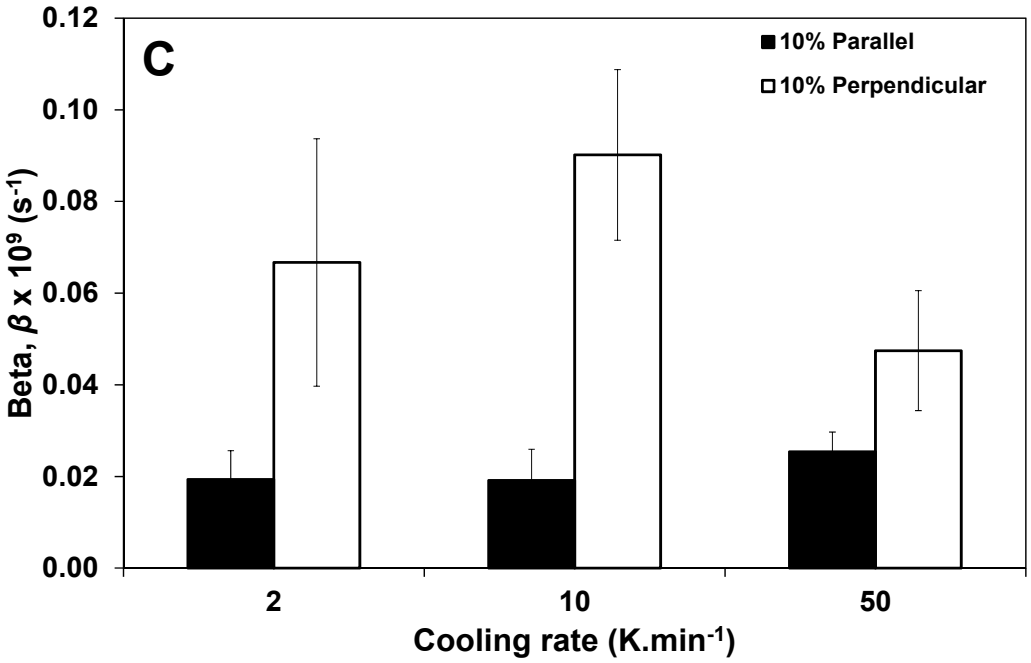
C
10% Parallel
10% Perpendicular
Beta, β x 10^9 (s^-1)
0.12
0.10
0.08
0.06
0.04
0.02
0.00
2
10
50
Cooling rate (K.min^-1)

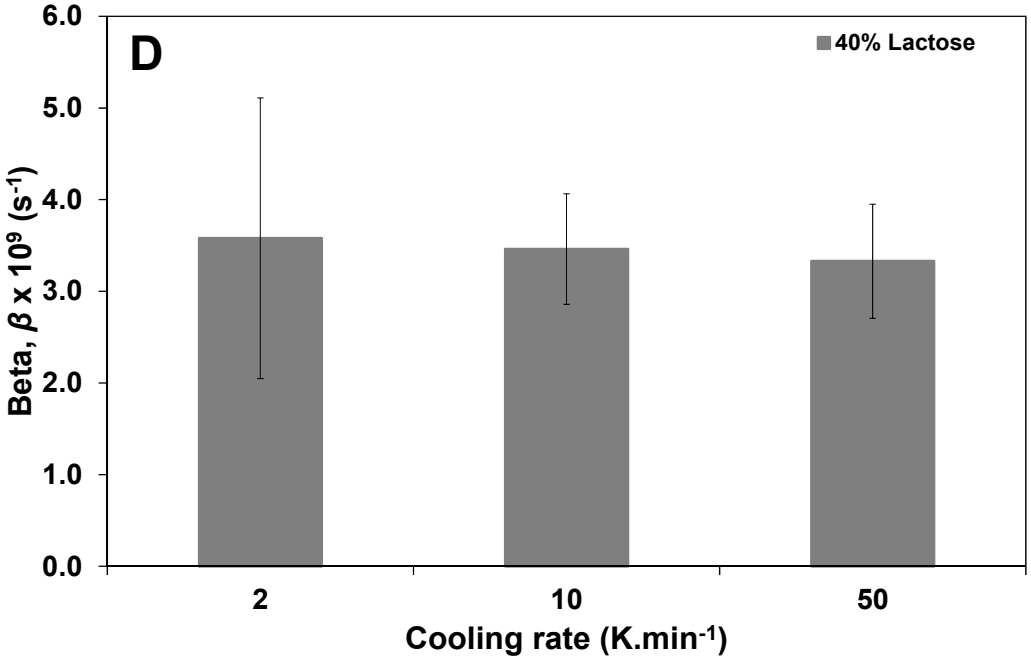
D
40% Lactose
Beta, β x 10^9 (s^-1)
6.0
5.0
4.0
3.0
2.0
1.0
0.0
2
10
50
Cooling rate (K.min^-1)

Figure 11

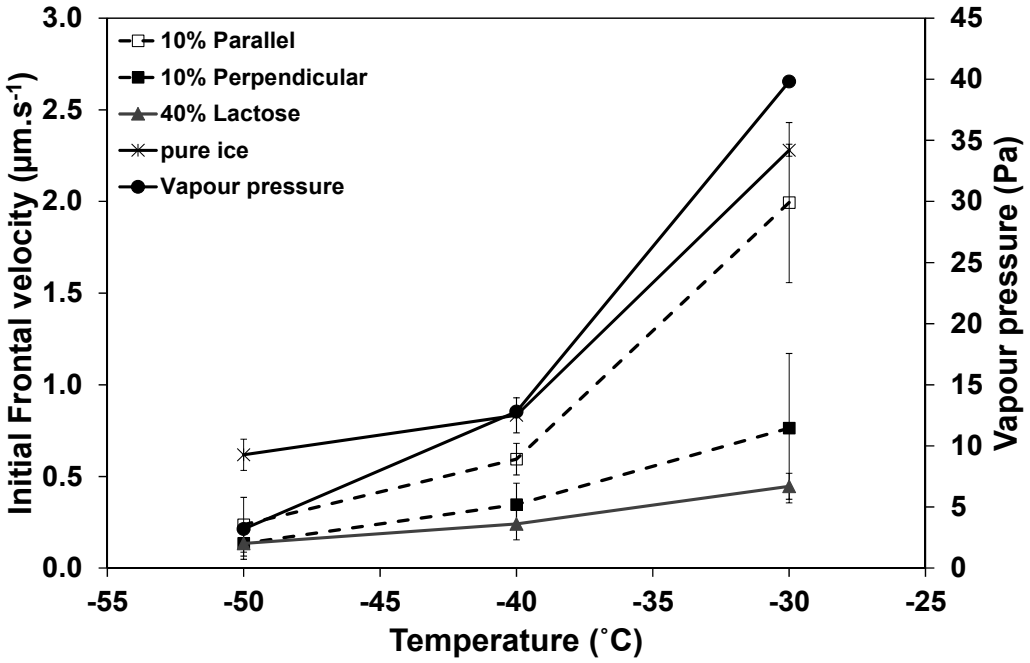
10% Parallel
10% Perpendicular
40% Lactose
pure ice
Vapour pressure
Initial Frontal velocity (µm.s-1)
Vapour pressure (Pa)
Temperature (˚C)
3.0
2.5
2.0
1.5
1.0
0.5
0.0
45
40
35
30
25
20
15
10
5
0
-55
-50
-45
-40
-35
-30
-25

Figure 12

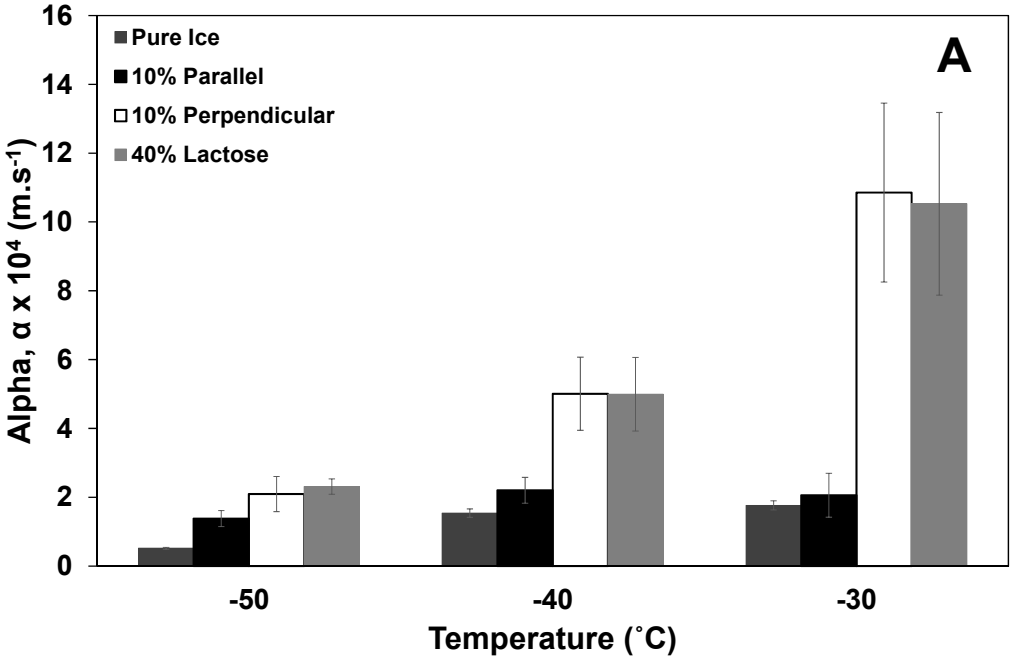
Pure Ice
10% Parallel
10% Perpendicular
40% Lactose
A
Alpha, α x 10^4 (m.s^-1)
16
14
12
10
8
6
4
2
0
-50
-40
-30
Temperature (˚C)

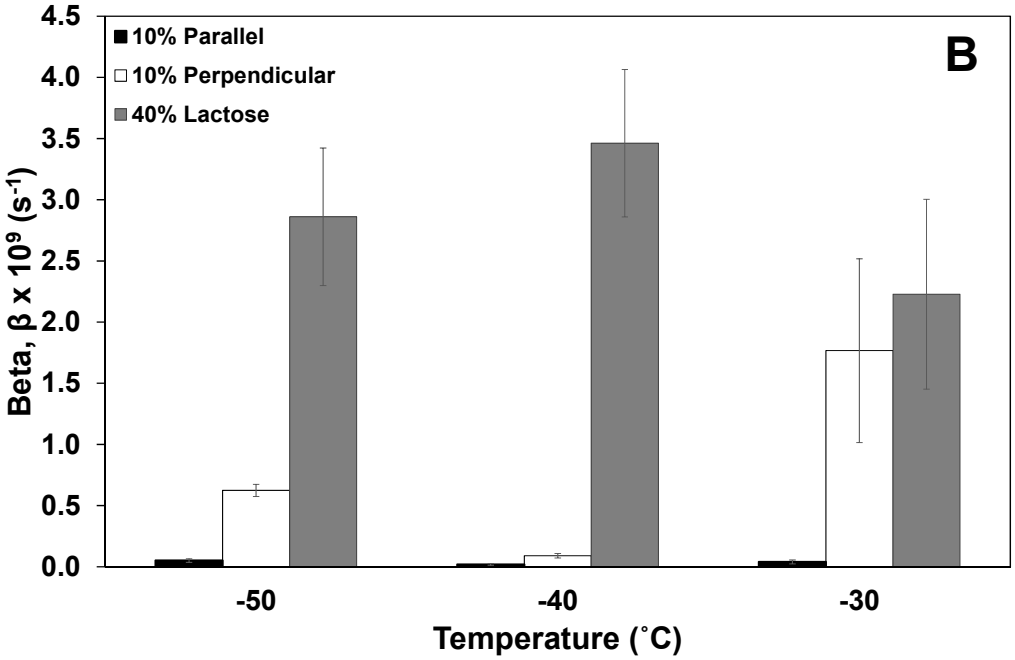
10% Parallel
10% Perpendicular
40% Lactose
B
Beta, β x 10^9 (s^-1)
4.5
4.0
3.5
3.0
2.5
2.0
1.5
1.0
0.5
0.0
-50
-40
-30
Temperature (˚C)

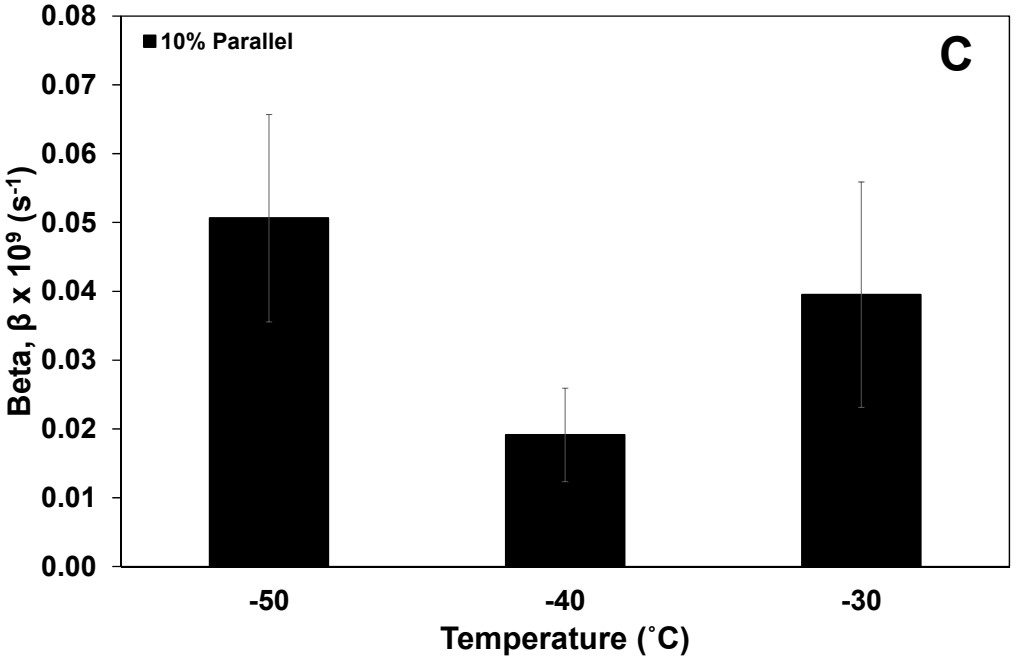
0.08
0.07
0.06
0.05
0.04
0.03
0.02
0.01
0.00
Beta, β x 10^9 (s^-1)
10% Parallel
C
-50
-40
-30
Temperature (˚C)

Figure 13

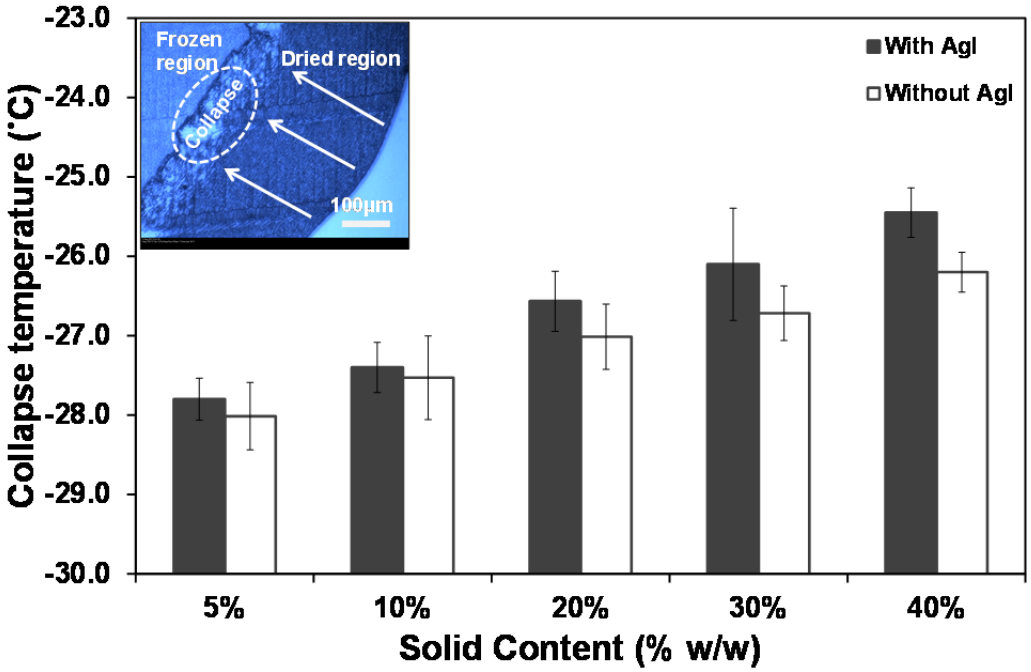
Frozen region
Dried region
Collapse
100µm
With AgI
Without AgI
Collapse temperature (°C)
-23.0
-24.0
-25.0
-26.0
-27.0
-28.0
-29.0
-30.0
5%
10%
20%
30%
40%
Solid Content (% w/w)

Figure 14